Segmental Dynamics in Poly(methylphenylsiloxane) Networks by Dielectric Relaxation Spectroscopy

Benjamin D. Fitz and Jovan Mijovic*

Department of Chemical Engineering and Chemistry, Polytechnic University, 6 Metrotech Center, Brooklyn, New York 11201

Received December 17, 1998; Revised Manuscript Received March 12, 1999

ABSTRACT: The segmental dynamics of PMPS chains are determined in the bulk liquid and cross-linked networks of varying cross-link density by broad-band dielectric relaxation spectroscopy. A large fragility index [$\tau(T_g^*/T)$ dependence], $F_{1/2} = 0.77$, is found, independent of cross-link density, molecular weight, and T_g. Also independent of the above variables is the relaxation shape (characterized by a KWW β parameter of 0.45). Since these parameters quantifying the α process in PMPS networks are insensitive to cross-linking, it is concluded that the length scale of cooperatively rearranging domains in PMPS networks is smaller than the distance between cross-links, i.e., less than 5 nm, in agreement with the current consensus. An argument based on the temperature dependence of the dielectric relaxation strength, dipole moment, and ensemble average chain configuration was advanced, suggesting that the high fragility of PMPS has an intramolecular origin.

Introduction

The dynamics of the segmental relaxation process (α relaxation) in chemically cross-linking networks has been the subject of recent interest.[1−9] A variety of cross-linking systems have been explored, ranging from highly cross-linked thermoset-forming epoxide/amine formulations[1,5−9] to rubbery-gel-forming polyurethanes,[4] to cross-linked copolymers,[3] to randomly cross-linked homopolymers via reactive side groups.[2] Missing from these studies has been the case of polymers cross-linked via reactive end groups. With such an approach the distance between cross-links may be directly controlled, allowing the inquisition of several fundamental dynamics characteristics, such as the length scale of cooperatively rearranging domains[10,11] and the primitive segmental correlation length.[12,13] Length scales for the cooperatively rearranging domain associated with the α process have been extracted from such diverse techniques as NMR,[14] atomic force microscopy,[15] calorimetry,[10] dielectric relaxation spectroscopy on polymers and molecular liquids confined within nanoporous glass,[16,17] confined thin-film liquids under shear,[18] probe molecule rotational/translational mobility differences,[19] dynamic and static light scattering,[20−23] spectral hole burning,[24] and molecular dynamics simulations.[25] The present consensus is that this length scale is approximately 2−5 nm.

Of the experimental techniques available for the study of relaxation processes in polymers, polymer networks, and low molecular weight glass-formers, dielectric relaxation spectroscopy (DRS) is rapidly becoming a dominant tool.[26] The molecular-level response probed, the wide frequency range available (12−14 decades), ease of sample preparation, and short measurement times are a few advantages. One of the limitations of DRS in the studies of molecular dynamics is that the material under study must contain a permanent dipole, though the type and concentration of dipoles can vary during cross-linking.

To systematize the various scenarios possible, we propose a classification scheme based on four general classes of cross-linking reactions that result in network formation and can be probed by DRS: *Class 1*: dipoles present in the reactants are not involved in the chemical reaction so that the product contains the same concentration (normalized for density changes) and type of dipolar groups (e.g., telechelic polymer chains with low-polarity reactive end groups and dipolar groups in the polymer backbone—such as vinyl-terminated siloxane polymers). *Class 2*: dipoles present in the reactants (not necessarily all of them) are involved in the reaction, and a new type of dipole is formed (e.g., a reactive mixture of epoxide- and amine-containing molecules which react forming secondary and tertiary amines and hydroxyl groups). *Class* 3: dipoles present in the reactants (not necessarily all of them) react to form nonpolar groups (e.g., cyanate ester resins which cross-link to form symmetric nonpolar triazine rings). *Class 4*: no dipoles are present among the reactants but are formed during the reaction (e.g., oxidation of polyethylene by radiation cross-linking). General examples of all of these classes are illustrated in Figure 1. The above scheme encompasses only systems that undergo *chemical* cross-linking and does not include physical cross-linking, hydrogen-bonded structures, reversible gels, etc.

Dynamics of a class 1 cross-linking system are under investigation in this paper. An ideal polymer network-forming system for such dynamics studies will meet the following criteria: simple molecular structure, lack of strong specific interactions, facile supercooling (in order to avoid complications due to crystallization), and well-characterized monomer or neat polymer segmental dynamics. A candidate polymer meeting those criteria is an end-group-functionalized poly(methylphenylsiloxane) (PMPS). Additionally, PMPS is an important polymer, with notable flexibility,[27] high-temperature stability, and tunable optical properties.

The objective of the present work is to investigate the reorientational dynamics of PMPS of both neat polymer and samples of varied cross-link densities. To characterize quantitatively the segmental dynamics, we use the

* To whom correspondence should be addressed.

10.1021/ma981937b CCC: $18.00
Published on Web 04/22/1999

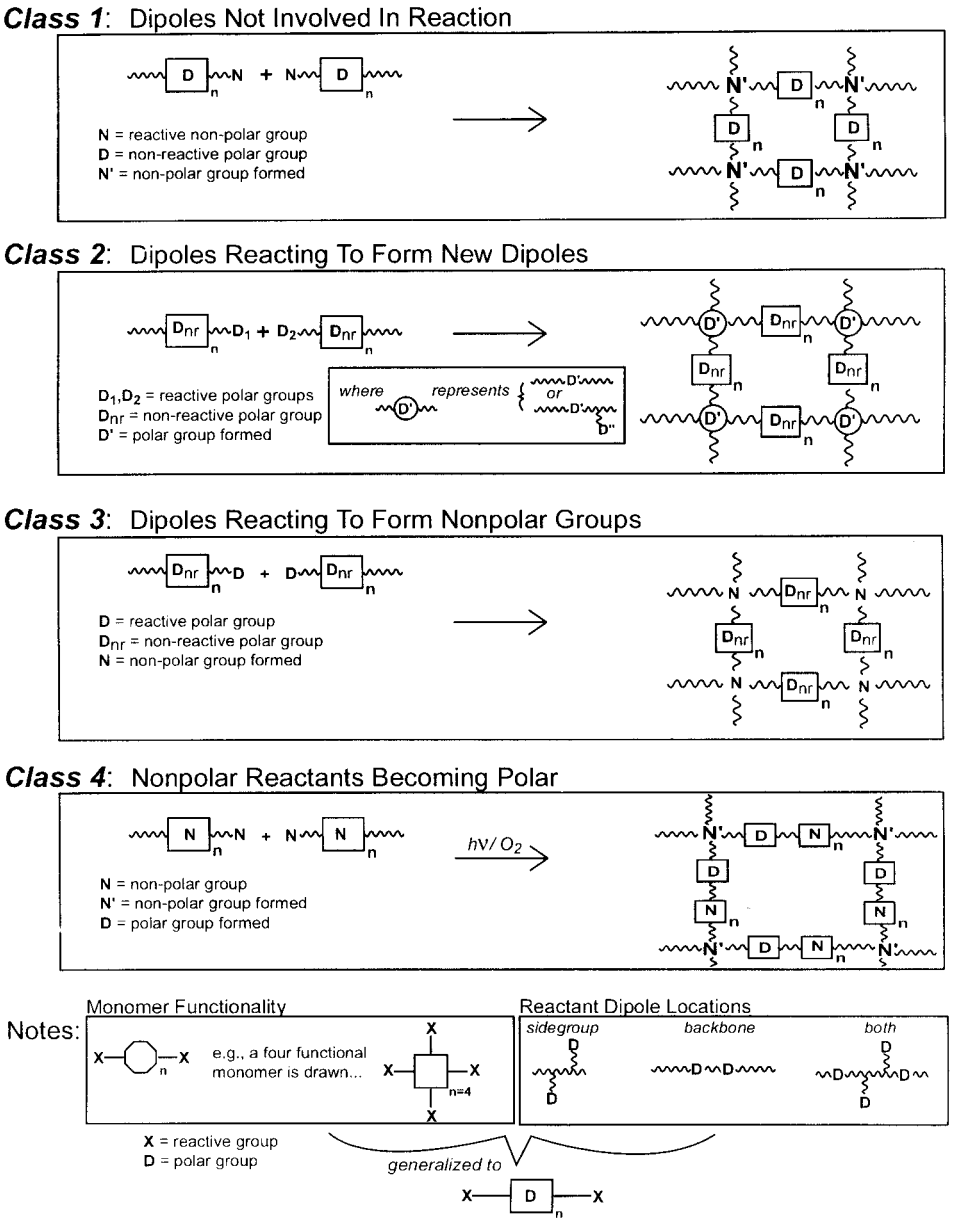

Figure 1. Classification scheme for dipolar group compositional changes during cross-linking.

conventional relaxation function and relaxation time temperature dependence models. We discuss the results in terms of cooperative and segmental length scales.

Theoretical and Experimental Background

Dielectric Relaxation Spectroscopy. The response of a material with permanent dipoles to an applied electromagnetic field can be written as a complex permittivity,[28,29] ϵ^* (in the frequency range where only dipole relaxations are occurring):

$$\frac{\epsilon^*(i\omega) - \epsilon_\infty}{\epsilon_0 - \epsilon_\infty} = 1 - i\omega\int_0^\infty \exp(-i\omega t)\phi(t)\,\mathrm{d}t \qquad (1)$$

where ω is angular frequency, ϵ_∞ is the dielectric constant at $\omega \gg \omega_{max}$ where ω is sufficiently high such that only atomic and electronic polarizations contribute (at $\omega >$ secondary β processes), and ϵ_0 is the static dielectric constant which contains the contributions of ϵ_∞ with the addition of polarizations due to permanent dipoles. $\phi(t)$ describes the polarization decay and is often modeled by eq 2, the Kohlrausch−Willams−Watts[30] (KWW) equation:

$$\phi(t) = C\mathrm{e}^{-(t/\tau)^\beta} \qquad (2)$$

where C is a constant, τ is the relaxation time, and β is a stretching exponent ranging from 0 to 1. Since we obtain ϵ^* in the frequency domain, we transform the relaxation kernel (eq 2) from the time domain into the frequency domain, using the technique described by Dishon et al.[30] and then fit the experimental data to the transformed kernel with appropriate parameters.

Alternatively, $\epsilon^*(\omega)$ may be modeled by a number of empirical functions, one of which was originated by Havriliak and Negami,[32] the HN function, given by

$$\epsilon^*(\omega) = \epsilon_\infty + \frac{\epsilon_0 - \epsilon_\infty}{[1 + (i\omega\tau_{HN})^a]^b} + i\frac{\sigma}{\omega^n\epsilon_v} \qquad (3)$$

where a and b are the dispersion shape parameters, σ is the conductivity, n accounts for deviations in migrat-

ing charge mechanisms, and ϵ_v is the vacuum permittivity. The other parameters are defined in eq 1.

We next briefly outline considerations for examining the temperature dependence of the relaxation times extracted from dielectric experiments via eqs 2 or 3.

Quantifying the Temperature Dependence of the Relaxation Time. Relaxation times for molecular dynamic observables, such as the apparent segmental dipolar reorientation time, τ_{max}, obtained in the dielectric experiment, depend very sensitively on temperature. Changes with temperature of τ_{max} range over 14 decades in time, reflecting the molecular dynamic extremes of the rapid dynamics in the liquid regime, to the very slow dynamics of structural relaxations in amorphous solids. Despite over 100 years of investigation, a consensus on the most appropriate form to quantify the behavior has not been reached. Several of the models have been recently reviewed by Richert and Angell[33] and by Stickel et al.[34] A starting point is the Arrhenius plot: a presentation of relaxation data in the form of $\log(\tau)$ vs $1/T$, which may be subsequently scaled to allow comparison of materials with differing T_g's by plotting $\log(\tau)$ vs T_g/T or occasionally $(T - T_g)/T_g$. It is well-known that the primary relaxation in glass-formers deviates from a thermally activated Arrhenius form—a more severe change in τ with decreasing temperature is usually found. Such behavior is often acceptably modeled by the empirical Vogel−Fulcher−Tammann (VFT) equation:[35]

$$\tau = \tau_0 \exp\left[\frac{E_a}{k(T - T_v)}\right] \tag{4}$$

where τ_0 is the high temperature−high frequency limit for τ, E_a is an apparent activation energy for the process, k is the Boltzmann constant, and T_v, the Vogel temperature, is a temperature below T_g where the relaxation is considered to be frozen—all of these parameters are usually taken to be fitting constants. Further interpretations and fundamental physical arguments resulting in the VFT form may be found in the literature.[36−38] A careful analysis of the model reveals that the VFT equation is not valid over the entire experimental temperature range for low molecular weight glass-formers.[34] However, for many polymers and glass-forming low molecular weight liquids the VFT form yields an adequate fit.[39,40] Whether a model fits experimental observation within objective criteria will, of course, depend on the objective criteria. There are two central issues to be considered as motivating factors for reorientational dynamics investigations: (1) a search for a general law for the $\tau(T)$ data for any glass-former typically with an intention of finding critical temperatures or temperature ranges (e.g., mode coupling theories[37])—in this case the most stringent objective criteria are required; and (2) a search for a method of obtaining a unique fingerprint or signature of the $\tau(T)$ behavior of a material so that different materials may be quantitatively compared and the parameters gained from such a method related to molecular characteristics. Naturally, less stringent objective criteria may be required if the models result in acceptably distinct "fingerprint" parameters.

Toward fingerprinting methods, several approaches have been advanced, all of which seek a unique, single indexing parameter, characterizing a material's $\tau(T_g/T)$ behavior. Since a single index is desired, scalings such as T_g/T are introduced to condense the parameters into one. Forms that directly fit $\tau(T)$ data have multiple parameters (e.g., VFT has three). We will follow the literature and generically refer to these indices as fragility[40] indices (one can also find them referred to as cooperativity[42] indices); we will be elaborating on the term fragility, shortly. A commonly used fragility index, also known as the steepness index,[45] is defined by

$$m = \frac{\mathrm{d} \log \tau_{max}}{\mathrm{d}(T_g/T)}\Big|_{T=T_g} \tag{5}$$

There are inherent difficulties in obtaining this slope at temperatures near T_g, where the largest experimental errors are found. (The relaxation times are near the instrumentation limits, temperatures are low and difficult to stabilize for the necessarily long measurement periods, and structural relaxation (physical aging) effects may undesirably contribute.) Another fragility index is F^*, defined by

$$F^* = \frac{T_v}{T_g} \tag{6}$$

which is obtained after fitting the experimental data to eq 5 (VFT) and also requires a determination of T_g. To compare F^* indices of different materials, it is recommended to fix the VFT τ_0 at the attempt frequency value of 10^{-14} s.[39] This index suffers from its link to the VFT model which, as previously mentioned, may not yield a sufficiently accurate fit. Recently, a new $\tau(T)$ benchmark, $F_{1/2}$, has been advanced by Richert and Angel.[33] The index is defined

$$F_{1/2} = 2\frac{T_g}{T_{1/2}} - 1 \tag{7}$$

where $T_{1/2}$ is defined by the relation

$$\tau(T_{1/2}) = 10^{-6}\ \mathrm{s}$$

The approach circumvents the limitations surrounding the previously mentioned steepness index, m. In this case, $F_{1/2}$ is obtained at temperatures and experimental frequencies that are within the range of greatest experimental confidence. Additionally, the T_g/T region where $F_{1/2}$ is determined is one in which differences in material τ values are greatest, so that a high degree of discrimination between materials with similar $\tau(T)$ dependencies can be made. Hence, $F_{1/2}$ is the fragility index we will use in our analysis. It should be noted that difficulties arise for this approach if an α/β crossover occurs in this 10^{-6} s region.

Attempts to connect the fragility indices to molecular characteristics have been made.[36,41,42] They are often summarized in simplified rules: the greater the index, the more fundamental relaxing structures (molecule, portion of molecule, cooperatively rearranging domain) in a material are subject to interactions (cooperativity[42]) and the more the liquid morphology, or liquid quasi-order,[38,43] is degraded with increasing temperature. A classic example of a material with a low fragility index (because of which it is called a strong glass-former) is silica glass, a highly coordinated inorganic network-former which remains quasi-ordered over a wide temperature range. A high-fragility index example is TMPC (tetramethylpolycarbonate),[45] having a highly temper-

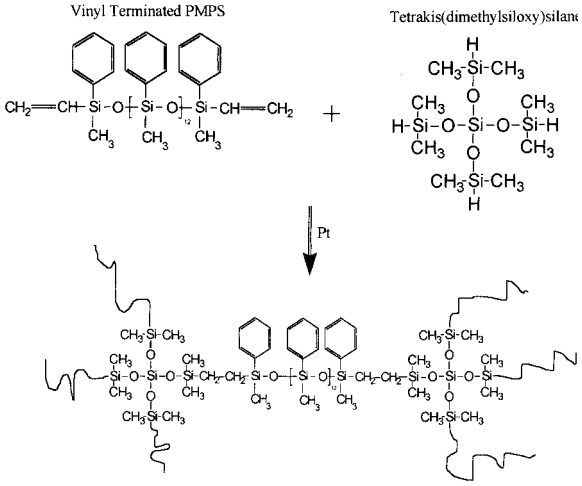

Figure 2. Network forming reaction of poly(methylphenylsiloxane).

ature-dependent segmental mobility attributed to the rigid, sterically hindering aromatic rings in the polymer backbone. As phrased by Roland and Ngai,[44] "...smoother, less polar, more compact, symmetric and flexible chemical structures, and those having less sterically-hindering pendant groups..." are those classifiable as low fragility/low cooperativity materials. These qualitative relations have been found to hold for a narrow range of polymers.[42] Although investigating these relations is not the focus of the present work, to clarify our findings on siloxane networks we have examined the relaxation dynamics of a wide range of materials, including polymers and molecular liquids. Our attempts to identify a pattern correlating molecular structure and fragility index are described below.

We reiterate that the primary aim of this investigation is to determine the influence of network connectivity on the α process $\tau(T)$ behavior and to inquire whether the above $\tau(T)$ models are sensitive to structural differences in polymer networks.

Experimental Section

Materials. The reactive polymer, vinyl-terminated poly(methylphenylsiloxane), PMPS, was obtained from Gelest, Inc. A schematic of the polymer network-forming reaction is shown in Figure 2. The cross-linker, tetrakis(dimethylsiloxy)siloxane, and catalyst, platinum cyclovinylmethylsiloxane complex, were obtained from United Chemical Technologies and were used as-received in the following preparation steps. The PMPS was washed in toluene, followed by precipitation in methanol. The polymer was then dried in a vacuum oven at 110 °C for 24 h. Size exclusion chromatography (SEC) was performed on a Waters (model 590) (in tetrahydrofuran at 1 mL/min, polystyrene calibration standards) where a weight-average molecular weight of ∼2200 g/mol and a number-average molecular weight of ∼1500 g/mol were found. (These values are approximate due to the use of polystyrene high molecular weight standards.) ^{1}H NMR (200 MHz) was used to ensure the purity of the polymer and also yielded an approximate agreement with the SEC number-average molecular weight (from the area under the vinyl and phenyl peaks, assuming the presence of no molecular cycles) for a value of 14 repeat units in the polymer. The glass transition temperatures for all of the polymer and various gel compositions were determined (DSC inflection point) on a TA Instrument Co. model 2920, with sample sizes of ∼10 mg and a heating rate of 10 °C/min; the T_g's are given in Table 1. By varying the concentration of the tetrafunctional cross-linker, we can control the cross-link density. The following compositions were used: (1) neat polymer (PMPS); (2) excess polymer 0.298% w/w to cross-linker (PMPS149), forming high molecular weight branched structures (but *nongelled*); (3) a stoichiometric mixture of polymer and cross-linker 7.48% w/w (PMPS374), this composition forming the tightest network structure; and (4) an excess of cross-linker 14.9% w/w (PMPS747), forming a network that is plasticized with cross-linker. The compositions were prepared, and the platinum-catalyzed hydrosilylation[46,47] reaction was carried out at room temperature with 0.02% w/w of catalyst complex. The reaction was followed by the disappearance of vinyl groups with mid-IR spectroscopy (Nicolet Magna 750, FTIR); for all compositions after 48 h the vinyl group absorbance reached a constant level, and the reaction was considered to be finished. The PMPS747 and PMPS374 samples form gels (as determined by visual inspection and handling of the reaction test tubes), while the PMPS149 sample is a highly viscous liquid.

Table 1. Temperature Dependence of Relaxation Time Parameters from VFT Fit and Fragility Indices for Several Indicated PMPS Network Compositions[a]

material	T_g[DSC] (K)	$T_{v,14}$ (K)	$E_{v,14}$ (eV)	τ_0 (s)	T_v (K)	E_v (eV)	$F_{1/2}$
PMPS	221	190.9	0.093	1.61e−15[b]	187.7	0.108	0.77
PMPS2	247	208.7	0.104	1.79e−14	210.2	0.098	0.76
PMPS149	227	198.0	0.090	3.96e−14	201.1	0.079	0.78
PMPS374	230	205.8	0.092	1.23e−13	210.4	0.074	0.78
PMPS747	224	192.7	0.097	6.96e−16	187.5	0.121	0.76

[a] $T_{v,14}$ and $E_{v,14}$ are from fits with $\tau_0 = 10^{14}$ (s); T_v and E_v are obtained with the corresponding fit value of τ_0. [b] Read as 1.61×10^{-15}.

Dielectric Relaxation Spectroscopy. A detailed description of our experimental facility for dielectric measurements is given elsewhere.[7] However, briefly, we have used a Solartron 1260 impedance/gain-phase analyzer to cover the frequency range 10^{-3} Hz to 10 MHz. This analyzer was used in conjunction with a high-impedance adapter of variable gain and a high-precision heating and cooling chamber, both from NOVOCONTROL, GmBH. From 1 to 1600 MHz an HP4291A impedance analyzer was used in conjunction with a sample cell, high-precision extension air line, and calibration software from NOVOCONTROL GmBH. An HP8752A network analyzer was used for the frequency range 10 MHz to 1.3 GHz, making use of our own modified sample cell and software to calculate the complex dielectric constant from the measured reflection coefficients.

Results and Discussion

Dielectric constant and loss were measured for each network composition across a wide frequency and temperature range. As the dielectric constant and loss are directly related via the Kramers−Kronig relations, for simplicity we present only the loss data in Figure 3. The solid curves are HN function best fits with the low-frequency conductivity contribution subtracted. The parameters are given in Table 2. There are no obvious trends in the HN *a* and *b* loss peak shape parameters (see Table 2); however, it is evident from Figure 3 that the HN function provides an adequate fit to the data.

Since the τ_{HN}, eq 3, is not equivalent to the apparent relaxation time (recall that the apparent relaxation time, $\tau_{app} = \tau_{max}$, is the reciprocal of the loss peak frequency (in radians) from the dielectric loss peak) for HN parameters a and $b \neq 1$, we must calculate it from the following relation:

$$\tau_{max} = \frac{1}{2\pi f_{max}} = \tau_{HN}\left[\sin\left(\frac{a\pi}{2+2b}\right)\right]^{1/a}\left[\sin\left(\frac{ab\pi}{2+2b}\right)\right]^{-1/a} \quad (8)$$

where the parameters are the same as in eq 3. The temperature dependence of τ_{max} for selected composi-

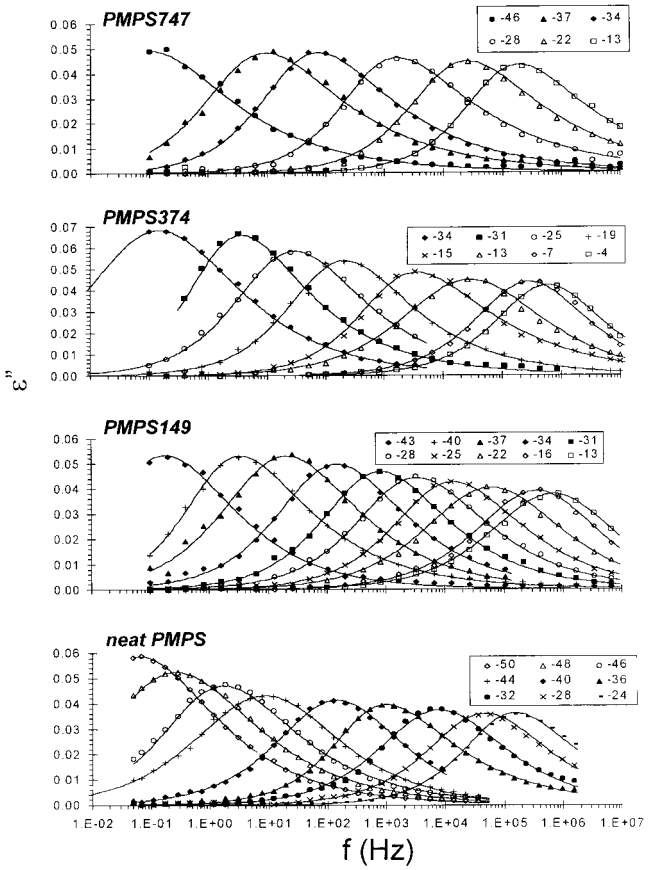

Figure 3. Dielectric loss in the frequency domain at specified temperatures for indicated compositions.

tions is shown in Figure 4. We include for comparison data of Boese et al.[48] on a higher molecular weight (~28 500 Da) linear PMPS sample. Also included are several high-frequency data points, for clarity not shown in Figure 3. The solid curves in Figure 4 are VFT fits; the corresponding parameters are listed in Table 1. Table 1 includes results from two versions of VFT fits: the first setting $\tau_0 = 10^{-14}$ s, yielding T_{v14} and E_{a14}, and the second with τ_0 free and the resulting parameters on the right-hand side of the table. While different PMPS networks have different T_g's, evidenced by the low-temperature τ_{max} behavior, the trends in the temperature dependence appear to be similar. This is verified when scaling τ_{max} by T_g^*/T (where T_g^* is the operational definition of T_g: the temperature at which τ_{max} is 100 s), as shown in Figure 5. The solid line in the main plot of Figure 5 is the Arrhenius limiting case. The inset of Figure 5 shows a magnified portion of the low-temperature region of the main plot. The solid curve in the inset and in the main plot is the VFT fit for the PMPS149 composition. (The VFT parameters from any of the other compositions generate curves with similarly good fits.)

It is of interest here to describe our procedure for generating Figure 5. Since our VFT fits with $\tau_0 = 10^{-14}$ s are excellent, we can evaluate T_g^* (the temperature at $\tau = 100$ s) by applying the fit VFT parameters and utilizing a rearrangement of the VFT equation:

$$T_g^* = T_v + \frac{E_a}{k(\ln \tau - \ln \tau_0)} \qquad (9)$$

where k is the Boltzmann constant, 86.2×10^{-6} eV/K, τ is 100 s, and τ_0 is 10^{-14} s. We note that in situations where the VFT fit is not as good significant error in extrapolation of τ to $T \rightarrow T_g$ will result, and as pointed out in the literature,[7,42] one must choose T_g^* to be a temperature where experimental data have been obtained. However, in that situation the fragility indices will not be comparable with those arrived at by the former method (T_g^*, $\tau = 100$ s) and will need to be recalculated using the new T_g^*.

We may quantify the temperature dependence of τ_{max} by any of the models discussed in the theory section. We have used VFT fits whose parameters are presented in Table 1. Additionally we have calculated a value for the steepness index, m, of 107, an F^* of 0.87, and an $F_{1/2}$ value of 0.77. These values place the polymer with materials such as propylene carbonate with an m of 104 and the binary mixture of toluene and chlorobenzene with an m of 107.[49] These materials are considered to be on the fragile end of the strong−fragile classification scheme (an exception at even higher fragility is PVC with an m of 200, though this value was obtained from a mechanical measurement).[53] We have also examined the data of Kirst et al.[51] on linear and cyclic PDMS chains and calculated the $F_{1/2}$ parameter, which is in agreement with our value of 0.77.

The question is raised whether the apparent high fragility of PMPS is significant and whether there are underlying molecular features that define a material as fragile or strong? To help answer this question, we examine dielectric relaxation data on a wide variety of materials, presented in the form of a relaxation map in Figure 6. This figure emphasizes the range of differences in $\tau(T_g^*/T)$ behavior for materials with widely differing molecular structures. The entries in Figure 6 include various polymers, the siloxane networks in the present study, and molecular liquids. Their chemical structures, VFT parameters, and fragility indices are summarized in Table 3. With the exceptions of 2 and 10, all other materials were measured in our laboratory. Clearly the PMPS polymers are among the more fragile materials; however, it is difficult to rationalize the similarity between the behavior of PMPS, PDMS (poly(dimethylsiloxane)), and some of the other materials with similar fragility, such as the molecular liquids DGEBA and MDA.[50] In fact, the similarity in fragility for PMPS and PDMS seems to be counter to the qualitative predictions set out in the Introduction. Since PMPS has a larger pendant group than PDMS (phenyl vs methyl), then based on the qualitative predictions an expectation of a significantly greater fragility should follow but is not found. While in the case of DGEBA and MDA, both are low molecular weight materials, their T_g's are nearly equivalent, each has a very similar aromatic center portion, both have the active dipoles on the end of the molecules, and both have a potential for hydrogen bonding. On the basis of that a priori molecular information, we may expect them to have similar fragility; this expectation is experimentally borne out. It remains unclear whether there can be any significance to the above four materials having very similar fragilities, since their molecular characteristics are quite different: polymer vs nonpolymer, hydrogen-bonding vs non-hydrogen-bonding, aromatic-containing (all except PDMS) vs non-aromatic-containing (PDMS), high-polarity (DGEBA) vs low-polarity (PDMS/PMPS), and with T_g's differing by 100 K. The factors governing fragility are

Table 2. Temperature Dependence of the HN Relaxation Function Fit Parameters at Selected Temperatures and PMPS/Cross-Linker Compositions

material	T (K)	σ (S/cm)	n	$\Delta\epsilon$	ϵ_∞	a	b	τ_{HN} (s)	τ_{max} (s)
PMPS	229	5.89e−16[a]	1.00	0.212	2.29	0.60	0.60	2.57e−2	1.87e−2
	251	6.16e−14	0.90	0.140	2.29	0.69	0.60	1.06e−6	5.45e−7
PMPS149	236	1.58e−14	0.80	0.220	2.28	0.59	0.67	1.44e−2	7.71e−3
	260	2.76e−12	0.85	0.150	2.28	0.56	0.98	2.34e−7	2.34e−7
PMPS374	242	3.13e−15	1.00	0.420	2.33	0.45	0.99	8.15e−2	8.15e−2
	269	1.10e−11	0.81	0.220	2.29	0.67	0.80	3.72e−7	2.76e−7
PMPS747	227	∼1e−20[b]	1.00	0.240	2.31	0.66	0.46	4.00e+0	1.38e+0
	260	1.12e−16	0.70	0.192	2.31	0.70	0.38	5.55e−7	1.81e−7

[a] Read as 5.89×10^{-16}. [b] Low sensitivity limit of instrument.

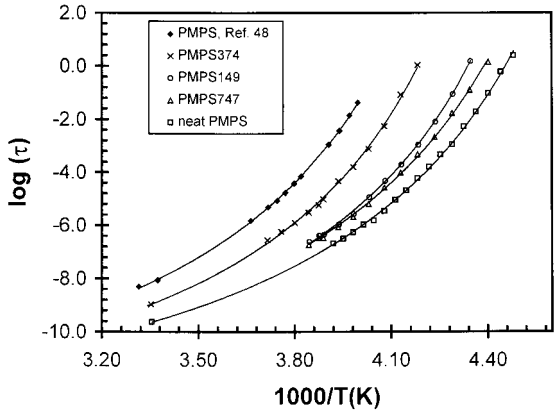

Figure 4. Temperature dependence of apparent relaxation time, τ_{max}, for all compositions.

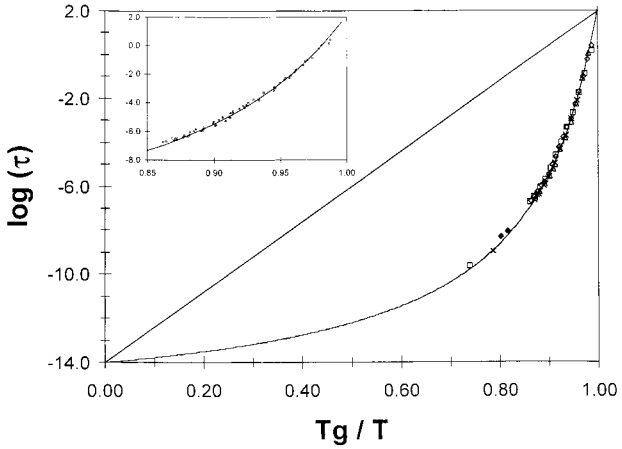

Figure 5. T_g/T scaled temperature dependence of apparent relaxation time, τ_{max}, for all compositions. Inset shows magnification of T_g/T range from 0.85 to 1.

obviously a confluence of inter- and intramolecular interactions, but a deconvolution of these interactions does not seem possible from the $\tau(T_g/T)$ behavior alone.

Despite the difficulty interpreting the fragility patterns, the siloxane polymers and networks in this investigation exhibit a larger fragility than would be expected for materials having a flexible Si−O backbone and a low T_g. In the following passages we consider several molecular explanations for the high fragility.

We first address the possibility that the fragility is correlated with secondary relaxations. The secondary process of interest is the phenyl ring flip. This process is not dielectrically active; hence, the low-temperature dielectric data (where secondary relaxations would be most noticeable) are featureless for all of the compositions. Another technique has been applied to the study of this process by Meier et al., who have observed the

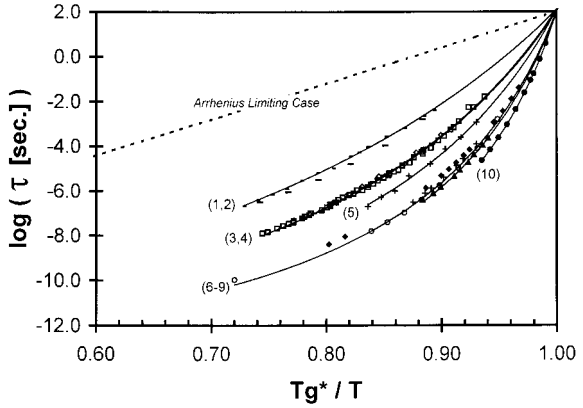

Figure 6. T_g/T scaled temperature dependence of apparent relaxation time, τ_{max}, for various polymers and molecular liquids; the numbers correspond to the materials in Table 3. The solid lines are VFT fits, and the parameters are given in Table 3.

phenyl flip mechanism via neutron scattering and NMR.[52] They found that the phenyl flip is coupled to the segmental α motion at high temperatures and decoupled at temperatures near and below T_g.[52] Temperatures near T_g are the most revealing of a materials fragility; therefore, since the phenyl flip is decoupled from the α process in this temperature range, the fragility is not correlated with it.

We next analyze the shape of the α process for both temperature and composition dependencies and seek its relation to fragility. We present in Figure 7master plots of the normalized dielectric loss for all of the compositions at selected temperatures. The solid curves are best-fit KWW functions. A contribution to the dielectric loss from conductivity is present at low frequencies; however, when ignoring the conductivity component, all four compositions have the same KWW fit β parameters of 0.45 (error ±0.01), indicating a cross-link-density-independent α relaxation distribution. We note that Boese et al.[48] also report a KWW β of 0.45 for their higher molecular weight, linear PMPS, measured by DRS and dynamic light scattering. A theoretical connection between fragility and relaxation shape has been advanced by Ngai et al., in terms of a coupling model[41] where the primitive relaxation is coupled to a "heat bath" and the relaxing segment cooperates with neighboring nonbonded segments, and separately by Vilgis[36] as an energy landscape model. Subsequently, the fragility to relaxation shape relations were experimentally verified,[45,53] indicating a strong positive correlation between these properties for many materials (there are a few exceptions[53]). The fragility/relaxation shape relation is also in agreement with the scaling work of Dixon et al.,[54] who showed that the relaxation width may be scaled with the temperature dependence of the relax-

Table 3. Temperature Dependence of Relaxation Time Parameters from VFT Fit and Fragility Indices for Several Polymers and Molecular Liquids

no. (Figure 6)	material	$E_{a,14}$ (eV)	$T_{v,14}$ (K)	T_g* (K)	$F_{1/2}$
1	glycerol	0.182	124.2	181.5	0.52
2	poly(acetaldehyde), ref 28	0.220	163.0	232.2	0.54
3	poly(vinyl acetate)	0.200	241.5	304.4	0.65
4	poly(propyleneoxide)	0.129	156.4	197.0	0.65
5	poly(methylhydrosiloxane)	0.066	103.1	123.8	0.71
6	PMPS	0.104	208.7	241.4	0.77
7	poly(dimethylsiloxane)	0.058	130.1	148.3	0.78
8	diglicidyl ether of Bisphenol A	0.098	223.5	254.3	0.78
9	methylenedianiline	0.094	224.5	254.0	0.79
10	poly(2-hydroxypropyl ether Bisphenol A), ref 63	0.114	331.5	367.3	0.82

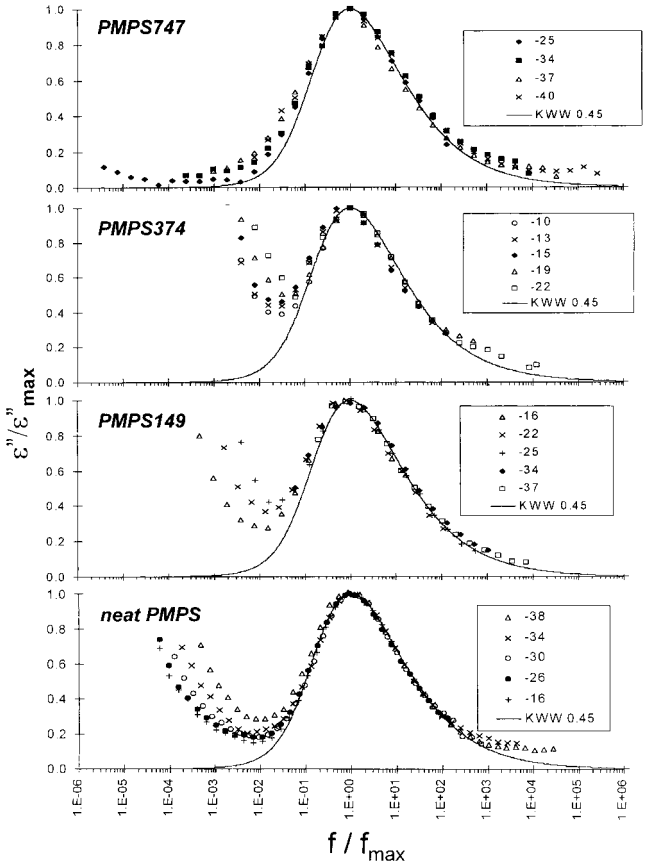

Figure 7. Normalized dielectric loss for the compositions specified in Figure 3.

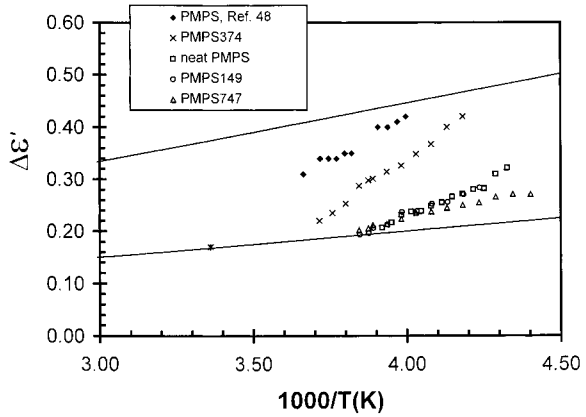

Figure 8. Relaxation strength for PMPS networks vs 1000/*T*.

ation time to generate a material-independent master curve. It is then not surprising that for the networks studied here, since no change in the relaxation shape is found for any of the cross-link densities tested, their fragilities are also invariant with cross-linking.

Finally, we examine the ensemble average molecular configurations of PMPS networks as a possible link to fragility. An additional piece of information obtained from DRS measurements is the relaxation strength, $\Delta\epsilon = \epsilon_0 - \epsilon_\infty$, related to chemical structure and ensemble average chain configuration through the dipole moment, μ. The temperature dependence of $\Delta\epsilon$ may then be used to find the temperature dependence of μ, which may offer additional insight on the fragility issue. The Onsager equation[29] establishes the connection between dipole moment and permittivity and is written

$$\langle\mu^2\rangle = \frac{9kTM}{4\rho\pi N_a}\frac{(\epsilon_0 - \epsilon_\infty)(2\epsilon_0 + \epsilon_\infty)}{\epsilon_0(\epsilon_\infty + 2)^2} \qquad (10)$$

where μ is the molecular dipole moment for an unassociated (freely rotating) molecule in the bulk liquid, k is the Boltzmann constant, T is the temperature, M is the molecular weight, ρ is the density, N_a is Avogadro's number, and ϵ_∞ and ϵ_0 are defined in eq 1. The definition of M and ρ in eq 10 must be redefined for a cross-linked network. We use the molecular weight between cross-links, i.e., the prepolymer molecular weight, and the prepolymer density.

The temperature dependence of $\Delta\epsilon$ is often difficult to unambiguously obtain due to a temperature-dependent overlap of α and β processes. However, since there is no dielectrically detectable secondary β process in these polymers, we were able to accurately collect these data and plot it versus 1000/T (K) in Figure 8. The two solid lines represent the Curie law: $\Delta\epsilon \propto 1/T$, each with a different slope. The Curie law holds if the individual dipolar orientations are uncorrelated. Since the relaxation strength for these PMPS polymers is changing more rapidly with temperature than either Curie law curve shown in Figure 8, the Si−O dipoles appear to be partially correlated. A plot of reduced permittivity (the rightmost factor on the rhs of eq 10) vs 1/T, shown in Figure 9, reveals that in fact the dipole moment is increasing with decreasing temperature. This interpretation is based on the following. The bounds for the slope of the reduced permittivity (given the behavior predicted by the Onsager equation, eq 10) are given by the solid lines in Figure 9. The experimental reduced permittivity slopes are too steep to be represented by eq 10, unless the dipole moment is increasing with decreasing temperature. The temperature dependence is $\mu = 0.85\cdot(1000/T\ [\mathrm{K}]) - 1.55$. From these data we calculate the mean-squared dipole moment relative to the dipole moment of a freely rotating chain (dipole moment ratio), $\langle\mu^2\rangle/nm^2$, where n is the number of skeletal bonds and m is the dipole moment of a skeletal bond. For our neat

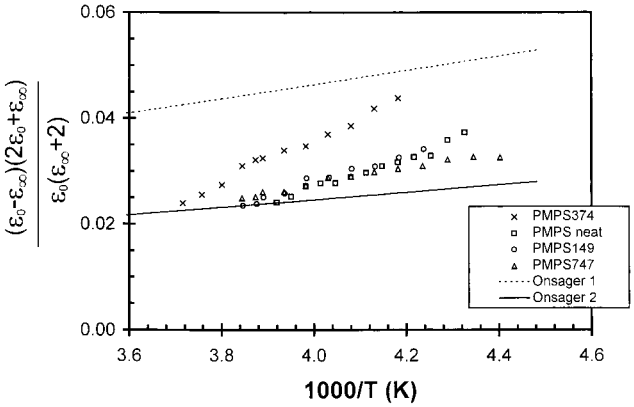

Figure 9. Reduced relaxation strength vs 1000/T.

PMPS sample, we obtain 0.26 at 25 °C, in good agreement with the value found by Salom et al.[55] of 0.28. A value less than one indicates hindered rotation around the Si−O skeletal bonds. In the above $\langle\mu^2\rangle$ calculations we use the density temperature dependence reported by Fytas et al.[56] on a similar molecular weight linear PMPS. Variations in density temperature dependence between our samples are not expected; moreover, they would not significantly affect the above calculations.

The Si−O unit dipoles apparently become more favorably aligned with decreasing temperature in all networks, although the degree of dipole correlation appears to be a complex function of cross-link density. For example, the highest cross-link density PMPS374 shows the greatest deviation from the Curie law, while the deviations in the other samples do not follow a simple monotonic law with decreasing cross-link density. As mentioned above, Salom et al.[55] have theoretically and experimentally obtained $\langle\mu^2\rangle/nm^2$ on neat PMPS chains at 25 °C. Their calculations were based on a rotational isomeric state (RIS) model,[57] which did not take into account intermolecular interactions. A similar study by Llorente et al.[58] showed an excellent agreement between RIS calculations (which also neglected intermolecular interactions) and strain birefringence measurements of the temperature coefficient of the unperturbed chain dimensions. One may then conclude that the excellent agreement found between experiment and the RIS calculations indicates that intermolecular interactions do not significantly influence the PMPS mean-squared dipole moment; the temperature dependence of $\langle\mu^2\rangle$ must have an intramolecular origin. An important intramolecular interaction was elucidated by Mark et al.[59] They applied the RIS model, calculated $\langle r_0^2\rangle/nl^2$ for PMPS chains, and found an attractive interaction between phenyl rings on adjacent skeletal silicon atoms. They found this unusual effect (contrary to vinyl polymers, where the adjacent pendant-group interactions are repulsive) to be due to the relatively long Si−O bond of 1.64 Å, and the large Si−O−Si bond angle of 143°, placing adjacent phenyl rings in the attractive region (separation of 3.8 Å for this pentane-type interaction) of the Lennard-Jones interaction potential. Another finding of the Mark study is that the temperature coefficient of $\langle r_0^2\rangle$ is positive, indicating a highly trans-favored isomerization at low temperatures. Flory et al.[60] reported that trans sequences are 0.85 kcal/mol lower in energy than gauche for PDMS polymer chains. These results suggest a qualitative prediction. On the basis of the PMPS chain geometry (cf. Figure 10) with increasing length of trans sequences, the resulting net

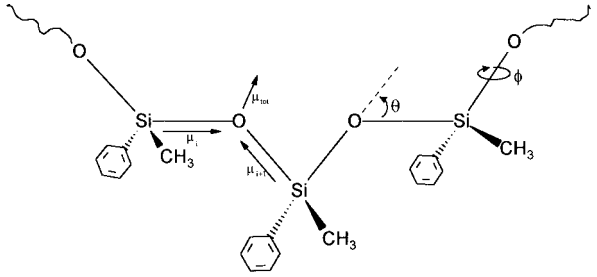

Figure 10. Illustration of planar all-trans chain configuration of PMPS. The bond angles and segmental dipole moments are indicated.

dipole moment of a given chain in such a configuration will decrease; for a closed planar cycle of 11 Si−O bonds the net dipole moment will vanish.[61] Thus, one expects that, by decreasing the temperature and increasing the trans population, the dipole moment should decrease. Our findings are at odds with this prediction. One possible explanation is that the molecular dipole moment (and corresponding chain configuration population) goes through a maximum with decreasing temperature. This maximum will be undetectable under the following circumstances. To obtain the relaxation strength, the relaxed component of the permittivity is required, but when the glass transition begins to set in, continued measurements of the relaxation strength to lower temperatures are prohibited and we are unable to reach sufficiently low temperatures to cross the maximum. It may prove interesting to investigate this aspect of the dipole moment of Si−O chains using computer simulations, which would not be constrained by the experimental glass transition. At this point we may conclude, on the basis of the relaxation strength (dipole moment) observations outlined above, that the high fragility in PMPS may have an intramolecular origin.

We would like to change the discussion now from the topic of fragility and focus our attention on the implications of changing cross-link density on the length scale of the segmental dynamics. First, recall that the fragility index of PMPS has been shown to be independent of cross-link density, molecular weight, and T_g. Also independent of these variables is the relaxation shape (characterized by a KWW β parameter). The fact that no change in the fragility index was found may not be significant, since several dissimilar materials were found to have equivalent indices. However, the fragility information taken together with the unchanged relaxation shape suggests the following conclusion. Since these segmental dynamic measures are not sensitive to the different PMPS structures examined, gels and linear chains, this implies that the relaxing segments are smaller than the distance between cross-links (~14 repeat units). An understanding of primitive segmental dynamics is, unfortunately, not directly accessible through a DRS test, as the dipole-containing segments are relaxing within cooperatively rearranging domains. It is not possible to predict how the domains ought to behave on the basis of molecular structure at present, although a recent attempt has been made.[12] Nevertheless, if the domain size distribution had been affected by cross-linking, one of the manifestations in a DRS test would be through the relaxation distribution (KWW β parameter). Since this is not the case for the PMPS networks here, we may infer that the characteristic domain size is smaller than the distance between cross-

links. In other terminology, although density fluctuations are quenched in regions very close to cross-links, fluctuations in density between the cross-links are not significantly disturbed—if the characteristic domain size were larger than this distance, upon cross-linking all fluctuations on this scale would be quenched, and only local (noncooperative) modes of relaxation would be observed.[62] We conclude that the distance between cross-links (~28 skeletal Si−O bond lengths, ~50 Å) is greater than the length of the primitive segment and the cooperatively rearranging domain; the length scale of the α process in PMPS networks is less than 5 nm. The upper length bound would be somewhat smaller than 5 nm if there is some immobilization near the cross-links. This size is in agreement with the value of about 2−5 nm, recently reported in several investigations of the cooperative length scale in polymers and molecular liquids.

Conclusions

The dynamics of PMPS chains were determined in the bulk liquid and cross-linked networks of varying cross-link density. The following findings were made. PMPS exhibits a large fragility index [$\tau(T_g^*/T)$ dependence], $F_{1/2} = 0.77$, which is independent of cross-link density, molecular weight, and T_g. Also independent of the above variables is the relaxation shape (characterized by a KWW β parameter of 0.45). On the basis of dipole moment observations, the high fragility of PMPS may have an intramolecular origin. Since the parameters quantifying the α process in PMPS networks are insensitive to cross-linking, it is concluded that the α length scale in PMPS networks is less than 5 nm. The α dynamics for a wide range of materials were contrasted with PMPS in a fragility (cooperativity) plot. There appears to be no obvious relation between molecular structure and the rate of change of the relaxation time when plotted in this manner.

Acknowledgment. This material is based on work supported by the National Science Foundation under Grant DMR-9710480.

References and Notes

(1) Deng, Y.; Martin, G. *Macromolecules* **1994**, *27*, 5141.
(2) Roland, C. M. *Macromolecules* **1994**, *27*, 4242.
(3) Glatz-Reichenback, J.; Sorriero, L.; Fitzgerald, J. *Macromolecules* **1994**, *27*, 1338.
(4) Tabellout, M.; Randriantoandro, H.; Emery, J.; Durrand, D.; Hayward, D.; Pethrick, R. *Polymer* **1995**, *36*, 4547.
(5) Fournier, J.; Williams, G.; Duch, C.; Aldridge, G. *Macromolecules* **1996**, *29*, 7097.
(6) Cassalini, R.; Livi, A.; Rolla, P. Levita, G.; Fioretto, D. *Phys. Rev. B* **1996**, *53*, 564.
(7) Fitz, B.; Andjelic, S.; Mijovic, J. *Macromolecules* **1997**, *30*, 5227. Andjelic, S.; Fitz, B.; Mijovic, J. *Macromolecules* **1997**, *30*, 5239. Andjelic, S.; Mijovic, J. *Macromolecules* **1998**, *31*, 8463.
(8) Wasylyshyn, D.; Johari, G. P.; Salvetti, G.; Tombari, E. *J. Phys.: Condens. Matter* **1997**, *9*, 10521. Ferrari, C.; Tombari, E.; Salvetti, G.; Johari, G. P. *J. Chem. Soc., Faraday Trans.* **1998**, *94*, 1293.
(9) Fitz, B.; Mijovic, J. Segmental Dynamics And Density Fluctuations in Polymer Networks During Chemical Vitrification. *Macromolecules*, in press.
(10) Donth, E. *J. Non-Cryst. Solids* **1982**, *53*, 325.
(11) Adam, G.; Gibbs, J. *J. Chem. Phys.* **1965**, *43*, 139.
(12) Matsuoka, S. *J. Appl. Polym. Sci.* **1997**, *64*, 77.
(13) Helfand, E. *Science* **1984**, *266*, 647.
(14) Schmidt-Rohr, K.; Spiess, H. *Phys. Rev. Lett.* **1991**, *66*, 3020.
(15) Russel, E.; Israeloff, N.; Walther, L.; Gomariz, H. *Phys. Rev. Lett.* **1998**, *81*, 1461.
(16) Floudas, G.; Paraskeva, S.; Hadjichristidis, N.; Fytas, G.; Chu, B.; Semenov, A. *J. Chem. Phys.* **1997**, *107*, 5502.
(17) Arndt, M.; Stannarius, R.; Groothues, H.; Hempel, E.; Kremer, F. *Phys. Rev. Lett.* **1997**, *79*, 2077.
(18) Hu, H.; Carson, G.; Granick, S. *Phys. Rev. Lett.* **1991**, *66*, 2758.
(19) Inoue, T.; Cicerone, M.; Ediger, M. *Macromolecules* **1995**, *28*, 3425.
(20) Fischer, E. *Physica A* **1993**, *201*, 183.
(21) Fischer, E.; Donth, E.; Steffen, W. *Phys. Rev. Lett.* **1992**, *68*, 2344.
(22) Debye, P.; Bueche, A. *J. Appl. Phys.* **1949**, *20*, 518.
(23) Moynihan, C. T.; Schroeder, J. *J. Non-Cryst. Solids* **1993**, *160*, 52.
(24) Schiener, B.; Bohmer, R.; Loidl, A.; Chamberlin, R. *Science* **1996**, *274*, 752.
(25) Mel'cuk, A.; Ramos, R.; Gould, H.; Klein, W.; Mountain, R. *Phys. Rev. Lett.* **1995**, *75*, 2522.
(26) Williams, G. In *Keynote Lectures In Selected Topics Of Polymer Science*; Riande, E., Ed.; CSIC: Madrid, 1997; Chapter 1, pp 1−40. Williams, G. In *Dielectric Spectroscopy Of Polymeric Materials*; Runt, J. P., Fitzgerald, J. J., Eds.; American Chemical Society: Washington, DC, 1997; Chapter 1, pp 3−65.
(27) Ferry, J. D. *Viscoelastic Properties Of Polymers*, 2nd ed.; Wiley: New York, 1980.
(28) McCrum, N. G.; Read, B.; Williams, G. *Anelastic and Dielectric Effects in Polymeric Solids*, Wiley: New York, 1967.
(29) Fröhlich, H. *Theory Of Dielectrics*, 2nd ed.; Oxford University Press: Oxford, 1958.
(30) Williams, G.; Watts, D. C. *Trans. Faraday Soc.* **1970**, *66*, 80.
(31) Dishon, M.; Weiss, G. H.; Bendler, J. T. *J. Res. Natl. Bur. Stand.* **1985**, *90*, 27.
(32) Havriliak, S.; Negami, S. *J. Polym. Sci., Part C* **1966**, *14*, 99.
(33) Richert, R.; Angell, C. A. *J. Chem. Phys.* **1998**, *108*, 9016.
(34) Stickel, F.; Fischer, E.; Richert, R. *J. Chem. Phys.* **1995**, *102*, 6251. Laughlin, W. T.; Uhlmann, D. R. *J. Phys. Chem.* **1972**, *76*, 2317. Barlow, A. J.; Lamb, J.; Matheson, A. J. *Proc. R. Soc. London, Ser. A.* **1966**, *292*, 322.
(35) Vogel, H. *Phys. Z.* **1921**, *22*, 645. Fulcher, G. *J. Am. Ceram. Soc.* **1923**, *8*, 339. Tammann, G.; Hesse, W. *Z. Anorg. Allg. Chem.* **1926**, *156*, 245.
(36) Vilgis, T. *Phys. Rev. B* **1993**, *47*, 2882.
(37) Goetze, W.; Sjogren, L. *Rep. Prog. Phys.* **1992,** *55*, 241.
(38) Jäckle, J. *Rep. Prog. Phys.* **1986**, *49*, 171.
(39) Angell, C. A. *Polymer* **1997**, *38*, 6261.
(40) Angell, C. A. In *Relaxations in Complex Systems;* Ngai, K. L., Wright, G., Eds.; National Technical Information Service, U.S. Department of Commerce; Springfield, VA, 1984.
(41) Ngai, K. L.; Rendell, R. W.; Rajagopal, A. K.; Teitler, S. *Ann. N. Y. Acad. Sci.* **1986**, *484*, 150.
(42) Ngai, K. L.; Roland, M. C. *Macromolecules* **1993**, *26*, 6824.
(43) Zallen, R. *The Physics Of Amorphous Solids*; Wiley: New York, 1989.
(44) Roland, C. M.; Ngai, K. L. *J. Non-Cryst. Solids* **1997**, *212*, 74.
(45) Plazek, D. J.; Ngai, K. L. *Macromolecules* **1991**, *24*, 1222.
(46) Momper, B.; Wagner, Th.; Maschke, U.; Ballauff, M.; Fischer, E. *Polym. Commun.* **1990**, *31*, 186. Valles, E.; Macosko, C. *Macromolecules* **1979**, *12*, 521.
(47) Warrick, E.; Pierce, O.; Polmanteer, K.; Saam, J. *Rubber Chem. Technol.* **1979**, *52*, 438.
(48) Boese, D.; Momper, B.; Meier, G.; Kremer, F.; Hagenah, J.; Fischer, E. *Macromolecules* **1989**, *22*, 4416.
(49) Angell, C. A. *J. Res. NIST* **1997**, *102*, 171.
(50) DGEBA, diglycidyl ether of Bisphenol A. MDA, methylenedianiline. These are a typical epoxy and amine thermoset-forming system (cf. ref 7).
(51) Kirst, K.; Kremer, F.; Pakula, T.; Hollingshurst, J. *Colloid Polym. Sci.* **1994**, *272*, 1420.
(52) Meier, G.; Fujara, F.; Petry, W. *Macromolecules* **1989**, *22*, 4421.
(53) Böhmer, R.; Ngai, K. L.; Angell, C.; Plazek, D. *J. Chem. Phys.* **1993**, *99*, 4201.
(54) Dixon, P.; Wu, L.; Nagel, S.; Williams, B.; Carini, J. *Phys. Rev. Lett.* **1990**, *65*, 1108.
(55) Salom, C.; Freire, J.; Hernandez-Fuentes, I. *Polym. J.* **1988**, *20*, 1109.
(56) Fytas, G.; Dorfmüller, Th.; Lin, Y.; Chu, B. *Macromolecules* **1981**, *14*, 1088.
(57) Flory, P. J. *Statistical Mechanics Of Chain Molecules*; Wiley: New York, 1969.

(58) Llorente, M.; Fernandez de Pierola, I.; Saiz, E. *Macromolecules* **1985**, *18*, 2663.
(59) Mark, J. E.; Ko, J. *J. Polym. Sci., Polym. Phys. Ed.* **1975**, *13*, 2221.
(60) Flory, P.; Crescenzi, V.; Mark, J. *J. Am. Chem. Soc.* **1967**, *86*, 146.
(61) Mark, J. *J. Chem. Phys.* **1968**, *49*, 1398.
(62) The phenomena of a network relaxation becoming entirely local because of the networks disturbance of the cooperative domain size is the subject of a future report from our laboratory. This effect is similar to the situation of amorphous polymer material confined within a thin space between crystalline lamellar walls, e.g. Schick, C.; Donth, E. *Phys. Scr.* **1991**, *43*, 423. A similar finding on PVDF/PMMA semicrystalline blends is also the subject of a forthcoming article from our laboratory.
(63) Alegria, A.; Guerrica-Echevarria, E.; Goitiandia, L.; Telleria, I.; Colmenero, J. *Macromolecules* **1995**, *28*, 1516.

MA981937B